Electron transport through a single InAs quantum dot

K. H. Schmidt,* M. Versen, and U. Kunze
Lehrstuhl für Werkstoffe der Elektrotechnik, Ruhr-Universität Bochum, D-44780 Bochum, Germany

D. Reuter and A. D. Wieck
Lehrstuhl für Angewandte Festkörperphysik, Ruhr-Universität Bochum, D-44780 Bochum, Germany
(Received 20 March 1999; revised manuscript received 17 July 2000)

InAs islands were embedded in the channel of an *n*-doped GaAs/AlGaAs high electron mobility transistor structure and a $60\times100\,\mathrm{nm}^2$ constriction was defined by lithography based on the atomic-force microscope and subsequent wet chemical etching. Compared to an unpatterned device a strong shift of the threshold voltage to higher gate voltages and well-defined peaks were observed at the onset of the conductance. The energetic position as well as the magnetic-field-induced shift of the peaks confirm that electron transport through the *p* shell of a single InAs quantum dot (QD) is observed. Our experimental data are in excellent agreement with calculations based on a simple parabolic quantum dot potential. A Coulomb blockade energy of ≈12 meV is determined for electrons in the first excited QD state.

I. INTRODUCTION

Zero-dimensional systems based on semiconductor materials have attracted more and more attention within the last decade. Those systems are not only interesting for improved device characteristics, they also allow the study of the behavior of electrons and holes in an atomiclike potential. In addition, all these investigations take place on an easy accessible energy scale. One of the most interesting material systems for research and applications are InAs self-assembled islands embedded in a GaAs matrix. Since these islands grow self-organized in the Stransky-Krastanow growth mode, their fabrication is relatively easy.[1–3] However, the biggest advantages of this system are the large confinement and Coulomb blockade energies caused by the small lateral and vertical extensions of the overgrown islands.[4–6] For an InAs quantum dot (QD) embedded in GaAs, a height of ≈4 nm and a radius of ≈15 nm is easily achievable.[7,8] Thus, many investigations have been done to get a better understanding of the growth,[1–3,9–11] and of the optical properties of this material system.[12–15] Recently several groups have also tried to study the electron transport characteristics of this QD system with capacitance[4–6,16] and tunneling spectroscopy.[17–22] A major problem of tunneling experiments is the fact that the QD levels have to be lifted above the GaAs band edge. In principle, there are two approaches to achieve such an energetic situation. For vertical transport experiments (perpendicular to the dot layer) the InAs islands were embedded in between two AlGaAs barriers.[17–19] However, the island formation on AlGaAs and the energetic position of the QD levels with respect to the GaAs conduction band edge are not well investigated, yet. In addition, since thin AlGaAs barriers are necessary for sufficiently high tunneling current signals, it is not certain that all the dots are totally capped with the barrier material.[8] Indium segregation makes the situation even worse.[23] Sharp lines were observed in such resonant tunneling experiments, which were attributed to tunneling through one big island, although thousands of dots were in the active region of the resonant tunneling diode. GaAs Schottky diodelike samples with InAs QD's embedded in an intrinsic GaAs layer between the doped back contact and the gate circumvent the problems mentioned above. Recently, tunneling through the *s* and *p* shell was observed in such structures.[24]

For in-plane tunneling experiments the islands were embedded in GaAs near the electron channel of a high electron mobility transistor (HEMT).[20–22] In combination with a split gate technique, lateral tunneling through more than 20 QD's was observed in such devices. However, due to the large number of QD's investigated in parallel, the interpretation of the *I-V* curves was again difficult.

In this paper we report on lateral tunneling experiments through the *p* shell of an individual InAs island embedded in GaAs. For these experiments the dot layer was positioned as close as possible to the electron channel of an *n*-doped AlGaAs/GaAs HEMT structure. In order to achieve tunneling through an isolated dot we used a lithographic technique based on the atomic-force microscope (AFM) and subsequent wet-chemical etching to define a point contact (PC) of about 60 nm length and 100 nm width. At a QD density of $\approx10^{10}\,\mathrm{cm}^{-2}$ there are at maximum three dots within the lithographically defined constriction. With increasing gate voltage sharp lines appear at the onset of the conductance which we attribute to electron transport through the *p* shell of a single InAs island. Due to the magnetic momentum of $m=\pm1$ a splitting of the tunneling features is observed when a magnetic field is applied to the sample in the growth direction. From the magnetic-field-induced shift we extract a Coulomb blockade energy of $E_C^p\approx12\,\mathrm{meV}$ for electrons in the first excited QD state. Our experimental findings are in excellent agreement with *CV* experiments, where the dots seem to be a bit smaller than the ones discussed in this paper.[6,12]

II. EXPERIMENT

The samples under investigation were grown in a RIBER EPINEAT III/V molecular-beam epitaxy (MBE) system on the semi-insulating GaAs substrate under an As beam

equivalent pressure of 1×10^{-5} Torr. For sample *A* and *B* a buffer sequence of 50 nm GaAs and a 150 nm thick GaAs AlAs (5 nm/10 nm) short-period superlattice were deposited to smooth out the surface roughness of the substrate. An intrinsic GaAs spacer layer of 625 nm separates the InAs system from the buffer layer. The substrate temperature was lowered from 630 down to 520 °C before 2.1 monolayer (ML) InAs were deposited with a growth rate of 0.02 ML/s. After an annealing time of 45 s the dots were capped with 8 nm GaAs before the temperature was ramped up again to 630 °C and additional 2 nm GaAs were grown. A 15 nm thick undoped $Al_{0.3}Ga_{0.7}As$ spacer layer suppresses the influence of the following Si δ-doped layer ($n\approx1\times10^{13}\,cm^2$) on the electrons in the *n* channel of the HEMT structure. Finally, the sample was capped with 10 nm Si-doped $Al_{0.3}Ga_{0.7}As$ ($n\approx10^{18}\,cm^3$) and 5 nm GaAs (Si $n\approx10^{18}\,cm^3$).

Hall measurements performed at $T=4.2$ K give an electron density of $n_e=5\times10^{11}\,cm^2$ in the channel of the transistor. Since the InAs QD's act as additional scattering centers the electron mobility is strongly reduced down to $\mu_e=1.8\times10^3\,cm^2/V\,s$.

For reproducibility purpose we processed additional nominal identical devices (sample *C* and *D*) on a second wafer grown under similar conditions. For this MBE material an electron density of $n_e=3\times10^{11}\,cm^{-2}$ and a mobility of $\mu_e=1.5\times10^3\,cm^2/V\,s$ was determined at low temperatures.

In order to check the influence of the dots on the transport characteristic of the patterned devices a third HEMT structure was fabricated without dots in the channel region. Due to the absence of the dots, the low-temperature mobility of this material increased to $\mu_e=1\times10^5\,cm^2/V\,s$ at a carrier density of $n_e=3\times10^{11}\,cm^{-2}$.

A mesa was etched and Ohmic source drain contacts were processed on each side. In order to study the quantum transport in samples *B*, *C*, *D*, and *E*, a constriction was defined on a mesa by AFM lithography and subsequent wet chemical etching between the source and drain contact [see Fig. 1(a), sample *E* is without dots in the channel]. Finally the etched area was covered with a Au Schottky gate to adjust the potential of the PC and the energy levels of the QD's with respect to the Fermi energy of the source contact. Details of the processing can be found in Refs. 25 and 26. Figure 1(b) shows a scanning electron microscope image of the metallized PC of sample *B*. The inset depicts a corresponding micrograph taken from a reference sample, where the QD's on the surface were grown under similar conditions used for the investigated HEMT structures. Due to the material contrast between GaAs and InAs, the InAs islands appear as bright spots. A dot diameter of ≈25 nm was determined for the uncapped islands. It can clearly be seen that at a dot density of $\approx1\times10^{10}\,cm^{-2}$, at maximum, 3 QD's fit into the constriction shown in the main frame of Fig. 1(b)

A sinusoidal source voltage of $\Delta U_S=0.5$ mV was applied to the sample and the drain current was measured as a function of the applied gate voltage with a standard lock-in technique [compare Fig. 1(a)]. The peak intensity of the transport features linearly increases with the modulation amplitude (checked up to $\Delta U_S\leqslant5$ mV), while their full width at half maximum remains constant for $\Delta U_S<1$ mV. Thus, at $\Delta U_S=0.5$ mV the data are taken in the linear regime. The lithographically defined constriction (Fig. 1) results in a saddle potential in the channel of the HEMT structure since the etched grooves affect the two-dimensional (2D) electron gas-like gate fingers under high reverse bias (see Ref. 27 and references therein).

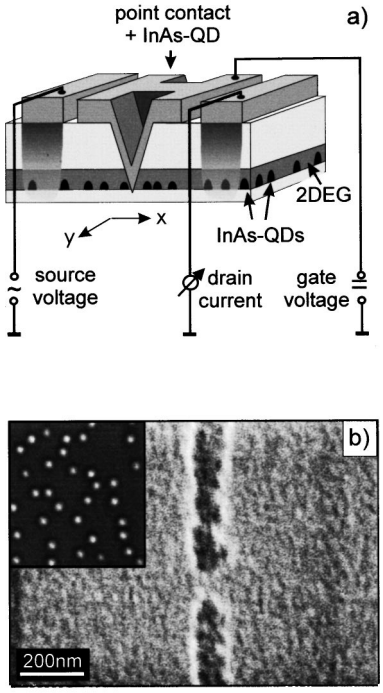

FIG. 1. (a) Schematic of the HEMT structure used for our single dot experiments. (b) displays a SEM image of the metallized PC region. The inset shows a SEM micrograph of InAs quantum dots grown on the surface of a reference sample.

A. Transport through a dot-free quantum point contact

In order to check the quality and functionality of our point contact we processed a patterned, as well as an unpatterned, HEMT structure based on a material without dots in the channel. Figure 2 displays the conductance measured on the dot-free samples *E* and *F*. The *I-V* trace of the unpatterned device (sample *E*) reflects the well-known characteristic of a field-effect transistor. When a negative bias is applied to the gate the channel is depleted and current flow between the source and drain contact is suppressed. Above the threshold voltage $U_{th}=-0.08$ V the channel is filled with electrons resulting in a smooth increase of the conductance signal at higher gate voltages until the δ-doped AlGaAs region comes into resonance with the Fermi energy and the conductance saturates.

The *I-V* characteristics of sample *F*, however, behaves completely different. A strong shift of the threshold voltage to higher gate voltages can be observed caused by the saddle potential in the constriction. In addition, the conductance signal shows a steplike increase which is characteristic for ballistic electron transport through a PC device.[27] The conductance is not exactly quantized by $2e^2/h$ due to additional series resistances but meanwhile exact quantization was achieved with similar devices.[28] It is important to note that all these measurements were done at $T=4.2$ K which demonstrates the excellent quality of our quantum point contact

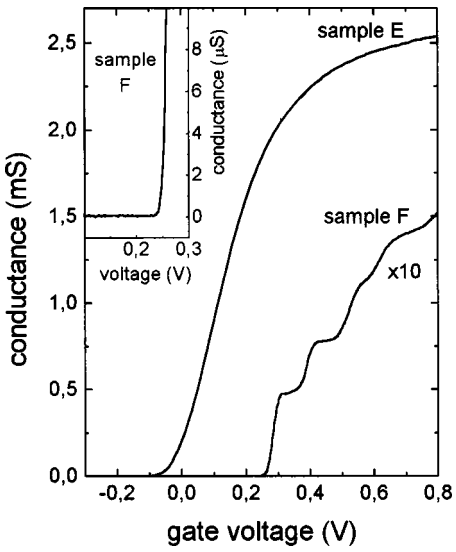

FIG. 2. Conductance signal of sample *E* and *F* measured at $T=4.2$ K with a modulation amplitude of $\Delta U_s=0.5$ mV. In contrast to the regular HEMT structure sample *E*, the signal of the quantum point contact device *F* is characterized by a steplike increase reflecting ballistic electron transport through 1D subbands. The magnified signal of sample *F* in the inset shows no peaklike structure.

devices and the large energy separation of ≈20 meV between the 1D subbands in the lithographically defined constriction.[28] The approximately constant gate voltage distance between adjacent conductance steps reflects the parabolic character of the saddle potential in the *y* direction (assuming a linear dependence of the Fermi level in the channel on the applied gate voltage). The blowup of the conductance of sample *F* demonstrates the sharp featureless onset of the signal between $0.1\,\mathrm{V}\leqslant U\leqslant 0.3\,\mathrm{V}$ (inset of Fig. 2). Again, this indicates the excellent quality of the PC and the smoothness of the saddle potential. In a trough-shaped potential electrons can be trapped in the tunneling regime and Coulomb blockade oscillations should occur at the onset of the *I-V* trace.

B. Single dot spectroscopy

If there is a QD in the constriction the potential drops in the InAs-rich region due to the band gap offset between InAs and GaAs (Fig. 3). Of course, Fig. 3 is only a schematic of the potential landscape. The real potential is more complicated due to strain effects and In/Ga alloying. Nevertheless, caused by the saddle potential environment the 0D levels of the QD in the constriction are lifted above the Fermi energy of the source and drain contact. By changing the gate voltage U_G the saddle potential of the PC and the energy levels of InAs QD's within the constriction are shifted relative to the Fermi energy of the source ($E_{F,S}$) and drain ($E_{F,D}$) contact (see Fig. 3). A peak appears in the conductance when a QD level comes into resonance with the Fermi level of the source contact and electrons are able to tunnel through the QD level from the source into the drain region. As soon as the QD level is shifted below $E_{F,D}$ the electron is trapped in the dot. In order to achieve tunneling again an additional gate voltage has to be applied to the sample to overcome the repulsive force of the trapped negative charge (Coulomb blockade).

Shapes of pyramids, cones, discs, and lenses (Ref. 29 and reference therein) have been reported for InAs islands em-

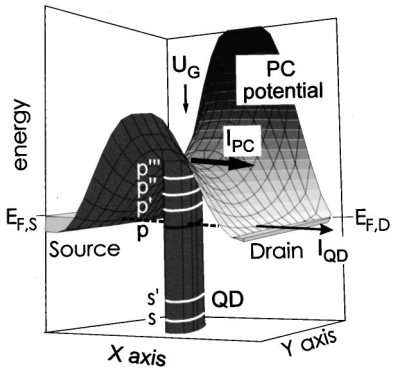

FIG. 3. Schematic of an InAs island in the center of the PC saddle potential. The 0D QD levels are labeled *s* and *s′* for the ground state and *p*, *p′*, *p″*, and *p‴* for the first excited state. The energy levels of each shell are separated by the Coulomb blockade energy. A tunneling current flows when the energetic position of a QD level is below the Fermi energy of the source contact $E_{F,S}$ and above the Fermi energy $E_{F,D}$ in the drain contact region (dashed arrow). At high gate voltages the saddle potential is shifted below $E_{F,S}$ and the electrons drift through continuum states giving rise to a continuum signal I_{PC}.

bedded in GaAs but the actual shape of the overgrown cluster is not unambiguously identified so far. However, the dots under investigation show the same electrical as well as optical behavior as the lens-shaped islands described in Refs. 4–6, 13, and 16. The 3D Hamiltonian of a lens-shaped QD can be separated into a component parallel and perpendicular to the dot layer.[12,30] Since the height of the overgrown islands is only a few nm,[31] the confinement in growth direction is very strong and only one bound state exists in the *z* direction. A simple two-dimensional parabolic QD potential seems to be good enough to roughly describe the electronic structure of the InAs islands in the lateral direction.[12,30,32,33] Since the energetic distance between the QD ground state and the wetting layer ground state is approximately 180 meV and the energy separation of 45 meV between adjacent dot levels is constant in a parabolic potential, we estimated 4 to 5 electronic levels in the QD.[5] This is also in good agreement with strain-induced photoluminescence measurements done by other groups.[34] However, due to Coulomb effects only the ground and first excited state can be investigated by capacitance spectroscopy[5,6,12] and by the experiments described in this paper.

Pauli's principle allows us to load each quantum level with two electrons. Consequently, two conductance peaks are expected for electron transport through the *s* shell (labeled *s* and *s′* in Fig. 2—Coulomb blockade effect). Since the degeneracy of the first excited state is twofold in the parabolic approximation, four resonances should be observable for the first excited state (labeled *p*, *p′*, *p″*, *p‴* in Fig. 2—Coulomb blockade plus degeneracy).

The main frame of Fig. 4 displays the conductance measured on the dot sample *A* and *B*, respectively. Since there are InAs islands in the channel region the conductance is strongly reduced in the unpatterned (sample *A*) as well as in the patterned device (sample *B*) compared to the samples without dots in the channel (see Fig. 2). As expected sample *A* shows the *I-V* trace of a regular HEMT structure since the lateral electronic coupling between adjacent QD's is weak

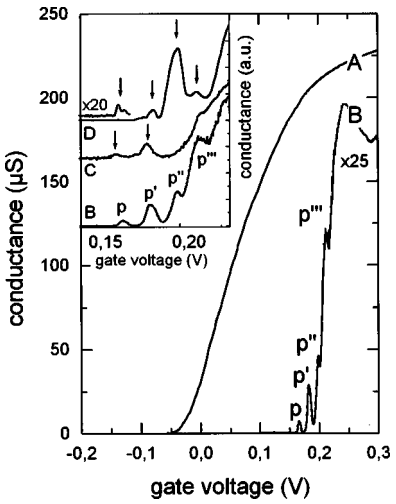

FIG. 4. Conductance of sample *A* and *B* measured at $T=4.2\,\mathrm{K}$ with a modulation frequency of $f=512\,\mathrm{Hz}$ and a modulation amplitude of $\Delta U_{SD}=0.5\,\mathrm{mV}$, respectively. The signal of sample *B* is multiplied by a factor of 25. The transport resonances through the Coulomb blocked first excited QD levels are labeled by p, p', p'', and p'''. The inset shows in detail the interesting gate voltage regime of sample *B* compared to the conductance of the reference samples *C* and *D*. The conductance of sample *D* is multiplied by a factor of 20 at low gate voltages. The voltage distance between adjacent arrows and the conductance peaks of sample *B* (labeled p,p',p'',p''') are approximately the same reflecting a constant Coulomb blockade energy of the investigated InAs-QD's.

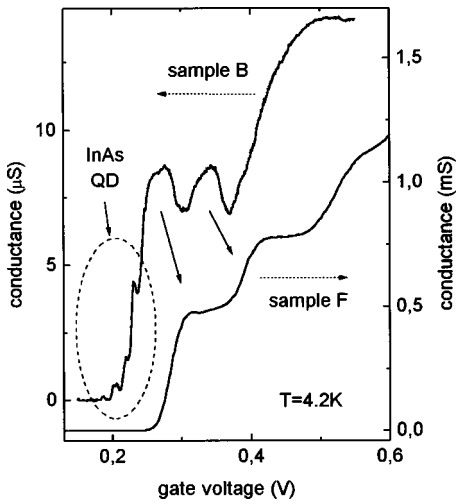

FIG. 5. Comparison between the conductance of sample *B* and *F*. The QD resonances are labeled by a dashed circle. The broad resonances in the *I-V* trace of sample *B* are attributed to electron transport through continuum states in the point contact (arrows).

and significant current flows only when the 2D level of the triangular-shaped channel potential is filled with electron. The *I-V* characteristics of sample *B*, however, behaves completely different. A strong shift of the threshold voltage to higher gate voltages can be observed caused by the saddle potential in the constriction (compare Figs. 2 and 3). In addition four sharp peaks (labeled p, p', p'', p''' in Fig. 4) appear at the onset of the conductance which are well reproducible at different cold cycles. Only a small gate voltage shift appears caused by a slightly different charge distribution in the surrounding of the constriction. However, the number and relative position of the peaks remain constant. Similar features can be found also in other PC devices with InAs QDs in the channel region. The inset of Fig. 4 displays the interesting gate voltage regime of sample *B* compared to the conductance signal of samples *C* and *D*. It is important to note that the gate voltage distance of $\Delta U_{p,p}\approx 17\,\mathrm{mV}$ between the tunneling features p and p' is roughly the same between all adjacent conductance peaks in samples *B*, *C*, and *D* (see also arrows in the inset of Fig. 4). This behavior reflects a nearly constant Coulomb blockade energy in all investigated QD samples and is also observed in other devices having only a few dots within the constriction.

Figure 5 directly compares the *I-V* signal of the QD sample *B* with the conductance of the dot free quantum PC device sample *F*. Since the *I-V* trace of sample *B* shown in Figs. 4 and 5 have been measured at different cold cycles, both figures nicely demonstrate the reproducibility of the QD transport resonances which appear right below the continuum signal (dashed circle). Due to the high scattering rate caused by the dots in the channel, the conductance of samples *B*, *C*, and *D* never reaches the ballistic regime. Thus, the continuum signal of the dot samples is much smaller than the ballistic signal of $2e^2/h=77\,\mu\mathrm{S}$. Consequently, in the QD devices it is not possible to observe the steplike increase of the PC conductance which is characteristic for ballistic electron transport through a 1D system (sample *F*). Instead, broad resonances characterize the continuum transport of sample *B* for $U>0.25\,\mathrm{V}$ (see Fig. 5). Their linewidth and their voltage separation is strongly increased compared to the peaks attributed to the InAs QD. We explain these features by electron transport through continuum states of the PC potential which are strongly modified by the QD in the center of the constriction (arrows in Fig. 5).

In contrast to the dot samples *B*, *C*, and *D* no peaked structure can be observed at the onset of the conductance of sample *F* (see also inset of Fig. 2). Since the nanolithographic processing was the same for all investigated PC samples, etching damages or tunneling through edge states cannot be responsible for the conductance peaks of samples *B*, *C*, and *D* between $0.15\,\mathrm{V}<U_G<0.25\,\mathrm{V}$ (Fig. 4). Thus, we attribute these resonances in the *I-V* trace to tunneling of electrons through the Coulomb-blocked shells of individual InAs QD's embedded in the PC potential.

The continuum signal of the PC shows no abrupt onset but gradually increases due to tunneling through the saddle point potential of the constriction (compare also the *I-V* trace of sample *E* between $0.25\,\mathrm{V}<U_G<0.3\,\mathrm{V}$ and of sample *C* between $0.2\,\mathrm{V}<U_G<0.24\,\mathrm{V}$ in Figs. 5 and 7, respectively). Since the energetic position of the QD levels is right below the continuum, the related transport resonances overlap with this featureless background and the signal does not go to zero between adjacent tunneling peaks.

In capacitance-voltage (CV) spectra taken on similar QD samples the charging of the ground (s shell) and first excited state (p shell) is clearly observable before charging of the wetting layer results in a strong increase of the capacitance signal.[5,12–16] According to these experiments the QD can be loaded at maximum with six electrons (two in the s shell, and four in the p shell). The features related to the tunneling into the s shell are separated by a Coulomb blockade energy of

$E_C^s \approx 20$ meV. For the *p* shell we expect four peaks which are approximately equidistant in energy (separated by the Coulomb blockade energy of $E_C^p \approx 12$ meV).[6,12] Due to confinement and Coulomb effects, the energetic distance between the Coulomb blocked *s*- and the lowest *p*-charging features is approximately $E_{sp} \approx 55$ meV.

Consequently, in our tunneling experiments we would expect two peaks at low gate voltages (tunneling through the *s* shell) then a voltage (energy) gap followed by four nearly equidistant peaks before electron transport through the continuum of the PC starts resulting in a more or less featureless current signal. In the other way round, when we leave the continuum and enter the tunneling regime with decreasing gate bias, we expect four equidistant peaks (tunneling through the *p* shell), then a gap and two additional peaks reflecting tunneling through the *s* shell. Since we only observe four equidistant peaks in the conductance of sample *B* right below the transport continuum, we relate these peaks to electron transport through the *p* shell of a single InAs QD. According to the strong decay of the tunneling features in Fig. 4 (caused by the increasing barrier heights at low gate voltages) electron transport through the *s* shell cannot be observed under our experimental conditions (it is expected at $U \leqslant 0.09$ V). This interpretation is in good agreement with Refs. 4 and 35 where charging of the QD ground state from a 3D electron reservoir through a triangular GaAs barrier was completely suppressed. In addition, magnetic-field experiments give also some evidence for this interpretation.

C. Magnetic-field dependence

Figure 6 displays the magnetic-field dependence of the conductance of sample *B*. At high magnetic fields the conductivity of the 2D electron gas in the source and drain contact regions is significantly modified and the resulting Shubnikov–de Haas oscillations interfere with the tunneling features discussed above ($U > 0.15$ V). In addition, caused by another experimental environment the spectra are more noisy and slightly shifted to lower voltages. However, the magnetic-field-dependent behavior of the transport feature labeled p' and p'' is clearly resolved (dashed arrows in Fig. 6). Since the voltage distance between the peaks increases with *B*, we assume that electron transport through the *p* shell (labeled *p* in Fig. 4) cannot be detected with the setup used for our *B*-field experiments. This statement will be justified later. The markers in the inset of Fig. 6 display the gate voltage position of peak p' and p'' versus magnetic field. The peaks are related to the position of resonance p' at $B = 0$ T. The data represented by the open and full symbols are taken at different cold cycles and demonstrate the reproducibility of the *B*-field shift of the peaks. The triangular markers display the voltage distance of resonance p' and p'' determined from Fig. 4. Since the magnetic momentum of the peaks is $m = \pm 1$, the related magnetic-field-induced shift of the conductance resonances is completely different.[6] While the feature labeled p' shifts to lower voltages with increasing magnetic field ($m = -1$), peak p'' ($m = +1$) remains approximately constant in energy, due to the magnetic-field dependence of the 2D emitter states. The solid lines in the inset of Fig. 6 display a fit of Fock-Darwin states to our experimental data. As already mentioned above the theory is

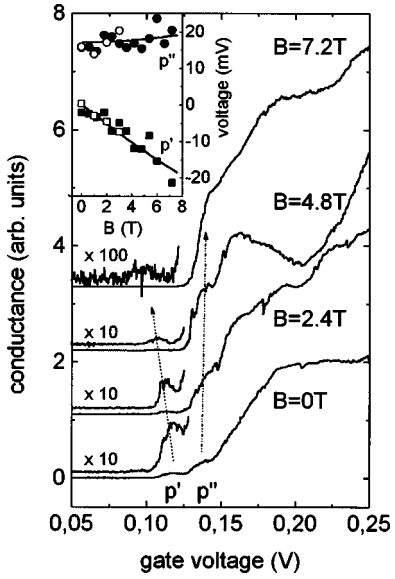

FIG. 6. Conductance of sample *B* measured at $B = 0$, 2.4, 4.8, and 7.2 T. An offset is added for clarity. At low applied gate voltages ($U < 0.13$ V) the signal is multiplied by factors of 10 and 100, respectively. The markers in the inset resemble the relative gate voltage positions $\Delta U_G(B)$ of the tunneling features p' and p'' with respect to the voltage position of p' at $B = 0$ T. Open and closed symbols are taken at different cold cycles. The triangular markers reflect the voltages distance of the equivalent levels p' and p'' taken from Fig. 4. The solid lines display the calculated magnetic-field dependence of Fock-Darwin levels fitted to the peak p' with a phenomenologically added shift of 17 mV arising from the Coulomb blockade.

based on a two-dimensional parabolic QD potential where the magnetic-field-induced energy shift (related to the energetic position $E_{1,-1}$ of shell p' at $B = 0$ T) is given by[36,37]

$$\Delta E_{N,m}(B) = (N+1)\hbar\Omega + m\hbar\frac{\omega_c}{2} - E_{1,-1}(B=0T) - \hbar\frac{\omega_c}{2},$$

$$N = n_+ + n_-, \quad m = n_+ - n_-, \quad n_+, n_- \in N_0, \qquad (1)$$

$$\Omega = \sqrt{\omega_0^2 + \omega_c^2/4}, \quad \omega_c = \frac{eB}{m^*}, \quad E_{1,-1}(B=0T) = 2\hbar\omega_0.$$

An energy between the *s* ($N = 0$) and *p* shell ($N = 1$) of $\hbar\omega_0 \approx 45$ meV was extracted from photoluminescence and capacitance experiments done on the same and similar samples.[5,12] Effective masses between $0.06 \cdot m_0 \leqslant m^* \leqslant 0.08 \cdot m_0$ (m_0 is the free-electron mass) are reported for electrons in InAs QD's.[6,12] Thus, we used the effective mass of GaAs bulk material ($m^* = 0.067 \cdot m_0$) in our calculations. The additional energy term $\hbar\omega_c/2$ in Eq. (1) reflects the influence of the magnetic field on the 2D electron gas in the source and drain contact, respectively. As soon as a magnetic field is applied in the growth direction, edge states are formed at the saddle potential of the PC.[38,39] The electrons are now emitted from the lowest edge state which shifts with $1/2\hbar\omega_c$ to higher energies in respect to the conduction band edge.

As already mentioned above the combination of quantum numbers $n_+ = 0$ and $n_- = 1$ results in an energy decrease of

the QD level p' with increasing magnetic field. The Coulomb blocked shell p'', however, is characterized by $n_+=1$ and $n_-=0$ and shows almost no magnetic-field dependence. Peak p' is well resolved in our experiments. So, we took its magnetic-field-induced energy shift $\Delta E_{1,-1}$ and the related change of the gate voltage position $\Delta U_{G,p'}(B)=U_{G,p'}(B)-U_{G,p'}(B=0T)$ to determine a transformation factor $\alpha=(1.47\pm0.13)/e$ from a fit between the calculated and the experimental data:

$$\Delta U_{G,p'}(B)=\alpha\cdot\Delta E_{1,-1}. \tag{2}$$

A conversion factor $\alpha\approx1.8/e$ was extracted from the temperature-dependent broadening of the transport feature labeled p in Fig. 4. This value is a bit higher than the one determined from magnetic-field experiments. However, the linewidths of the QD resonances of samples B and C are not only affected by temperature. For $\alpha=1.8/e$ a full width at half maximum of only $\Delta U=\alpha\cdot3.52\cdot k\cdot T=2.3\,\mathrm{mV}$ should be observed at $T=4.2\,\mathrm{K}$.[40] The experimentally determined value for samples B and C is $\Delta U\approx5\,\mathrm{mV}$. Due to tunneling times of $10^{-11}\,\mathrm{s}$, lifetime broadening can be neglected ($\approx10\,\mu\mathrm{eV}$). We attribute this additional broadening to enhanced Coulomb scattering at the potential of the charged QD's in the channel of the 2D emitter system. An electron mobility of $\mu\approx0.2\,\mathrm{m^2\,V\,s}$ results in an energy fluctuation of $\Delta E\geqslant\hbar/2\tau=\hbar e\mu/2m^*\approx4\,\mathrm{meV}$. The resulting broadening of $\Delta U\approx1.8\times4\,\mathrm{meV}/e\approx7\,\mathrm{mV}$ is in good agreement with our experimental findings. Since the temperature dependence of this mechanism is not known, it is difficult to extract a reliable conversion factor from activation measurements.

The variation of the source modulation amplitude results in a conversion factor of $\alpha\approx1.53/e$ (for a dot in the center of the constriction and neglecting any series resistances), which is similar to the one determined by magnetic field and activation measurements. From the gate voltage separation $\Delta U_{p,p'}\approx17\,\mathrm{mV}$ between the conductance peaks p and p' in Fig. 4 it is possible to extract a Coulomb blockade energy of $E_C^p\approx12\,\mathrm{meV}$ for electrons in the QD p shell ($\alpha=1.47/e$, from magnetic-field experiments). This is in excellent agreement with the value determined experimentally and predicted theoretically by other groups.[6,12] The magnetic-field-dependent behavior of the Fock-Darwin levels p''

$$\Delta U_{G,p''}(B)=\alpha\cdot(\Delta E_{1,1}+E_C^p), \tag{3}$$

also agrees reasonably well with our measured data (inset of Fig. 6). However, since the experimentally observed peaks are superimposed to an increasing background signal (compare Fig. 3), it is difficult to determine their exact gate voltage position.

In our magnetic-field measurements the conductance signal through the p shell of the QD seem to be below the detection limit of our experimental setup. The intensity drop of peak p' with increasing magnetic field confirms this interpretation. Since the QD level p' shifts to lower energies, the height of the tunneling barriers increases with magnetic field. This results in a decreasing tunneling probability and finally p' vanishes for $B>7.2\,\mathrm{T}$ (Fig. 6). Consequently, an energy shift of $\Delta E>13\,\mathrm{meV}$ (equivalent to a voltage shift of $\Delta U>20\,\mathrm{mV}$, $\alpha=1.47/e$) of the QD level p' is enough to suppress the tunneling current. Since the energetic distance between the QD level p and p' is of the same order of magnitude, electron transport through the p shell should be hardly resolvable. The QD ground state is even lower in energy (energetic distance between the s and p shell is approximately 45 meV). Thus, lateral tunneling through the s shell cannot be observed in this configuration.

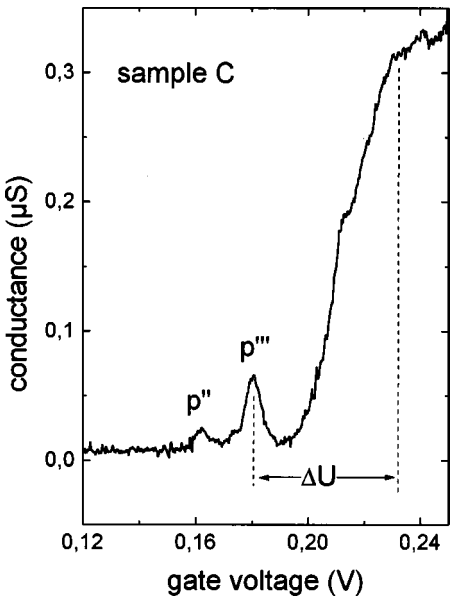

FIG. 7. Conductance of sample C measured at $T=4.2\,\mathrm{K}$ with a modulation frequency of $f=512\,\mathrm{Hz}$ and a modulation amplitude of $\Delta U_{SD}=0.5\,\mathrm{mV}$.

D. Multi-dot spectroscopy

Now, we focus on the transport characteristic of devices C and D (inset of Fig. 4). The conductance of sample C shows a large voltage gap ΔU between the last pronounced tunneling feature (labeled p''') and the continuum signal (Fig. 7). This effect can be explained by an asymmetric position of the QD in respect to the center of the PC potential (see Fig. 8). When the QD is positioned, for example, on the left slope of the saddle potential its 0D states are lowered in energy by ΔE^C compared to a QD in the center of the constriction. Consequently, the energy distance ΔE between the uppermost QD level p''' and the PC continuum is also increased (and with it the gate voltage difference $\Delta U=\alpha\cdot\Delta E$). However, due to the asymmetric position of the QD, the thickness as well as the height of the tunneling barrier on the right side of the dot is increased (compare Fig. 8). Thus, electron transport is only observable through the dot levels p'' and p''', respectively, and the intensity of the related conductance signal is strongly reduced.

With this interpretation it is also possible to explain the unusual relative intensities of the individual conductance peaks of sample D. While in samples B and C the peak intensity gradually increases with the gate voltage (reflecting the decreasing tunneling barrier at higher gate voltages), the conductance of sample D behaves completely different. Transport resonances 1, 2, and 3 in Fig. 9 gradually increase in intensity. The tunneling current of peak 4, however, is strongly reduced. Additionally, at least transport resonance 1 and 2 of sample D seem to consist of a set of narrow peaks next to each other.

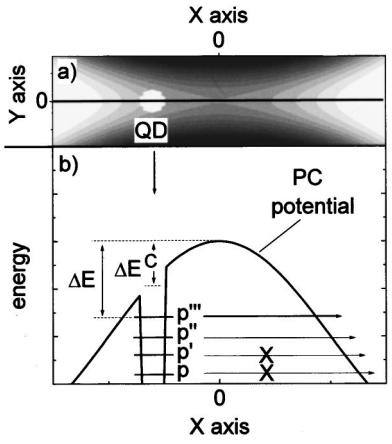

FIG. 8. (a) Schematic gray scale graphic of the saddle potential of sample *C* with a QD in the constriction. The position of the dot is slightly shifted to the left out of the center of constriction. (b) shows the PC potential along the solid line shown in (a). Compared to a QD in the center of the constriction the dot potential shown here is lowered in energy by ΔE^C. Due to the barrier height ΔE electron tunneling is possible only through the QD levels p'' and p''' [arrows in (b)].

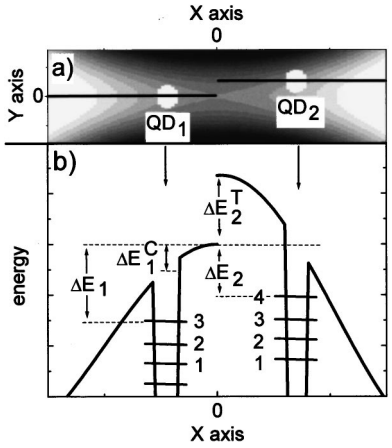

FIG. 10. (a) Schematic gray scale graphic of the saddle potential of sample *D* with two QD's in the constriction. The positions of the dots are slightly shifted to the left (QD_1) and to the right (QD_2) out of the center of constriction. (b) depicts the PC potential through QD_1 and QD_2 along the solid lines shown in (a), respectively. The QD levels responsible for the conductance peaks in Fig. 7 are labeled with 1–4.

This behavior can be explained by the dot distribution shown in the intensity plot of the PC potential sketched in Fig. 10(a). Since QD_1 is slightly shifted to the left out of the center of the PC, its 0D levels are lowered in energy by ΔE_1^C compared to a centered dot (see schematic potential at negative *x* values in Fig. 10). Consequently, less gate voltage is necessary to achieve tunneling through the energy levels of QD_1. However, a large gap $\Delta U_1 = \alpha \cdot \Delta E_1$ appears in the conductance after level 3 of QD_1 is shifted below the Fermi energy of the source contact and before the electrons are able to drift from the source to the drain region through the PC continuum (Fig. 9). Thus, the transport characteristic of QD_1 is similar to the one already discussed in sample *C*.

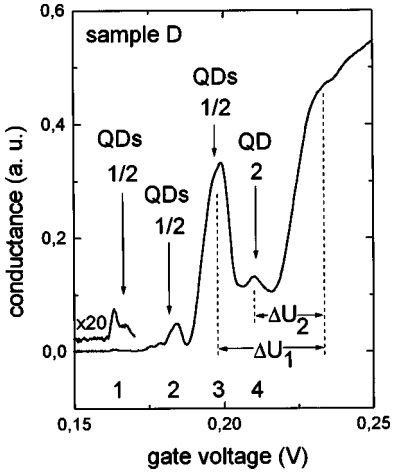

FIG. 9. Conductance signal of sample *D* ($T = 4.2$ K, $f = 272$ Hz, $\Delta U_{SD} = 0.2$ mV). The signal is multiplied by a factor of 20 at low gate voltages. The arrows mark the tunneling resonances (labeled 1–4) caused by QD_1 and QD_2, respectively. ΔU_1 and ΔU_2 describe the distance between the PC continuum signal and the tunneling resonance 3 and 4, respectively.

QD_2 seems to be positioned close to an equipotential line defined by the center of the PC potential since its uppermost tunneling resonance (labeled 4 in Figs. 9 and 10) is right below the PC continuum ($\Delta U_2 = \alpha \cdot \Delta E_2$ in Fig. 9). A position in the center of the saddle potential is very unlikely due to the low intensity of the transport resonance. Thus, we assume that QD_2 is shifted slightly to the edge of the PC (Fig. 10). In this case the tunneling barrier is enhanced by ΔE_2^T and the thickness of the left barrier is strongly increased compared to a centered QD. Both lead to a low intensity of the tunneling features assigned to QD_2. These considerations are also valid if electrons tunnel from QD_2 through the center of the PC potential. Since tunneling through level p_1', p_1'', and p_1''' of QD_1 [labeled 1, 2, 3 in Fig. 10(b)] takes place at approximately the same gate voltages as tunneling through p_2, p_2', and p_2'' of QD_2 [labeled also 1, 2, 3 in Fig. 10(b)], the intensity of the related tunneling features is enhanced (see Fig. 9). However, the peaks in the conductance are dominated by the electron transport through QD_1 due to a reduced tunneling barrier height compared to QD_2 ($\Delta E_1 < \Delta E_2 + \Delta E_T$). This interpretation is confirmed by magnetic-field experiments since the voltage position of the transport resonances 2, 3, and 4 in Fig. 7 are independent of an applied magnetic field up to 3 T. So far, QD1 and QD2 were considered independently. However, as already mentioned above each resonance QD1/2 in Fig. 9 consists of a set of narrow lines. In contrast to the electron transport through one QD in the constriction (sample *B* and *C*), these lines seem to be only thermally broadened. Activation measurements result in a conversion factor of $\alpha = 1.6/e$ which is in good agreement with the values already discussed in paragraph *C*. We attribute the fine structure to coupling phenomena between the energy levels of QD1 and QD2.[41] Since the narrow lines are grouped together, these effects seem to be weak compared to the observed Coulomb blockade energy of 12 meV. This is in good agreement with ensemble measurements. In capacitance experiments Coulomb blockade effects are well resolved and the observed broadening is dominated

by the size distribution of the dots and not by electrostatic effects of charging one dot on the electronic structure of an adjacent one.[42] The electronic coupling (formation of molecular states) between the QD's is also weak since absorption (photocurrent) and emission (photoluminescence) spectra reveal the same line shape reflecting again the size distribution of the dots. Thus, the probability of interdot carrier relaxation is low.[10]

III. CONCLUSION

In conclusion AFM lithography and subsequent wet chemical etching were used to define a narrow PC of $60\,\text{nm}\times 100\,\text{nm}$ in a *n*-doped HEMT structure. While an unpatterned device shows a smooth field effect transistor characteristic, a strong shift of the threshold voltage and pronounced peaks at the onset of the conductance were observed in the etched sample. These transport features are well reproducible and can be observed also in other PC devices with InAs QD's in the channel region. We attribute the transport resonances to electron tunneling through the *p* shell of individual InAs QD's within the lithographically defined constriction. Electron transport through the QD ground state is not observable under our experimental conditions. The magnetic-field-dependent shift of the peaks confirms our interpretation and is reproduced well by calculations based on a simple parabolic quantum dot potential.

ACKNOWLEDGMENTS

The financial support by the Deutsche Forschungsgemeinschaft (GK 384) is gratefully acknowledged.

*Corresponding author: Dr. Klaus Schmidt, Address: Werkstoffe der Elektrotechnik, Ruhr-Universität Bochum, D-44780 Bochum, fax: +49 234 32 14166, email address: schmidt@lwe.ruhr-uni-bochum.de

[1] D. Leonard, K. Pond, and P. M. Petroff, Phys. Rev. B **50**, 11 687 (1994).
[2] Q. Xie, A. Madhukar, P. Chen, and N. P. Kobayashi, Phys. Rev. Lett. **75**, 2542 (1995).
[3] S. Fafard, Z. R. Wasilewski, C. N. Allen, D. Picard, P. G. Piva, and J. P. McCaffrey, Superlattices Microstruct. **25**, 87 (1999).
[4] G. Medeiros-Ribeiro, J. M. Garcia, and P. M. Petroff, Phys. Rev. B **56**, 3609 (1997).
[5] K. H. Schmidt, G. Medeiros-Ribeiro, M. Oestreich, P. M. Petroff, and G. H. Döhler, Phys. Rev. B **54**, 11 346 (1996).
[6] B. T. Miller, W. Hansen, S. Manus, R. J. Luyken, A. Lorke, J. P. Kotthaus, S. Huant, G. Medeiros-Ribeiro, and P. M. Petroff, Phys. Rev. B **56**, 6764 (1997).
[7] B. Legrand, B. Grandidier, J. P. Nys, D. Stiévenard, J. M. Gérard, and V. Thierry-Mieg, Appl. Phys. Lett. **73**, 96 (1998).
[8] J. M. Garcia, T. Mankad, P. O. Holtz, P. J. Wellman, and P. M. Petroff, Appl. Phys. Lett. **72**, 3172 (1998).
[9] G. S. Solomon, J. A. Trezza, A. F. Marshall, and J. S. Harris, Jr., Phys. Rev. Lett. **76**, 952 (1996).
[10] K. H. Schmidt, G. Medeiros-Ribeiro, U. Kunze, M. Hagn, G. Abstreiter, and P. M. Petroff, J. Appl. Phys. **84**, 4268 (1998).
[11] L. Chu, M. Arzberger, G. Böhm, and G. Abstreiter, J. Appl. Phys. **85**, 2355 (1999).
[12] R. J. Warburton, C. S. Dürr, K. Karrai, J. P. Kotthaus, G. Medeiros-Ribeiro, and P. M. Petroff, Phys. Rev. Lett. **79**, 5282 (1997); R. J. Warburton, B. T. Miller, C. S. Dürr, C. Bödefeld, K. Karrai, J. P. Kotthaus, G. Medeiros-Ribeiro, P. M. Petroff, and S. Huant, Phys. Rev. B **58**, 16 221 (1998).
[13] K. H. Schmidt, G. Medeiros-Ribeiro, and P. M. Petroff, Phys. Rev. B **58**, 3597 (1998).
[14] K. H. Schmidt, G. Medeiros-Ribeiro, J. Garcia, and P. M. Petroff, Appl. Phys. Lett. **70**, 1727 (1997).
[15] S. Raymond, J. P. Reynolds, J. L. Merz, S. Fafard, Y. Feng, and S. Charbonneau, Phys. Rev. B **58**, R13 415 (1998).
[16] H. Drexler, D. Leonard, W. Hansen, J. P. Kotthaus, and P. M. Petroff, Phys. Rev. Lett. **73**, 2252 (1994).
[17] M. Ghisoni, O. Sjölund, and A. Larsson, Appl. Phys. Lett. **69**, 1773 (1996).
[18] M. Narihiro, G. Yusa, Y. Nakamura, T. Noda, and H. Sakaki, Appl. Phys. Lett. **70**, 105 (1997).
[19] A. S. G. Thornton, T. Ihn, P. C. Main, L. Eaves, and M. Henini, Appl. Phys. Lett. **73**, 354 (1998).
[20] K. Yoh, J. Konda, S. Shiina, and N. Nishiguchi, Jpn. J. Appl. Phys., Part 1 **36**, 4134 (1997).
[21] J. Phillips, K. Kamath, T. Brock, and P. Bhattacharya, Appl. Phys. Lett. **72**, 3509 (1998).
[22] N. Horiguchi, T. Futatsugi, Y. Nakata, and N. Yokoyama, Appl. Phys. Lett. **70**, 2294 (1997).
[23] H.-W. Ren, M. Sugisaki, S. Sugou, K. Nishi, and Y. Masumoto, J. Surf. Anal. **3**, 1 (1998).
[24] K. H. Schmidt, M. Versen, C. Bock, U. Kunze, D. Reuter, and A. D. Wieck, Physica E (to be published).
[25] B. Klehn and U. Kunze, J. Appl. Phys. **85**, 3897 (1999).
[26] S. Skaberna, M. Versen, B. Klehn, U. Kunze, D. Reuter, and A. D. Wieck, Ultramicroscopy **82**, 153 (2000).
[27] M. Büttiker, Phys. Rev. B **41**, 7906 (1990).
[28] S. Skaberna, U. Kunze, D. Reuter, and A. D. Wieck (unpublished).
[29] X. Z. Liao, J. Zou, X. F. Duan, D. J. H. Cockayne, R. Leon, and C. Lobo, Phys. Rev. B **58**, R4235 (1998).
[30] A. Wojs, P. Hawrylak, Phys. Rev. B **53**, 10 841 (1996).
[31] J. Garcia, T. Mankad, P. O. Holtz, P. J. Wellman, and P. M. Petroff, Appl. Phys. Lett. **72**, 3172 (1998).
[32] A. Wojs, P. Hawrylak, Phys. Rev. B **55**, 13 066 (1997).
[33] K. H. Schmidt, G. Medeiros-Ribeiro, U. Kunze, and P. M. Petroff, *Proceedings of the Fifth International Symposium on Quantum Confinement: Nanostructures*, 1998, Boston, MA, edited by M. Cahay (Electrochemical Society, Pennington, NJ, 1999), PV 98-19, pp. 213–227.
[34] I. E. Iskevitch, M. S. Skolnick, D. J. Mowbray, I. A. Trojan, S. G. Lyapin, L. R. Wilson, M. J. Steer, M. Hopkinson, L. Eaves, and P. C. Main, Phys. Rev. B **60**, R2185 (1999).
[35] R. J. Luyken, A. Lorke, A. O. Govorov, J. P. Kotthaus, G. Medeiros-Ribeiro, and P. M. Petroff, Appl. Phys. Lett. **74**, 2486 (1999).
[36] V. Fock, Z. Phys. **47**, 446 (1928).
[37] C. G. Darwin, Proc. Cambridge Philos. Soc. **27**, 86 (1930).
[38] P. C. Main, A. S. G. Thornton, R. J. A. Hill, S. T. Stoddart, T. Ihn, L. Eaves, K. A. Benedict, and M. Henini, Phys. Rev. Lett. **84**, 729 (2000).

[39] D. B. Chklovskii, B. I. Shklovskii, and L. I. Glazman, Phys. Rev. B **46**, 4026 (1992).
[40] C. W. J. Beenakker, Phys. Rev. B **44**, 1646 (1991).
[41] M. Tewordt, H. Asahi, V. J. Law, R. T. Syme, M. Kelly, D. A. Ritchie, A. Churchill, J. E. F. Frost, R. H. Hughes, and G. A. C. Jones, Appl. Phys. Lett. **60**, 595 (1992).
[42] G. Medeiros-Ribeiro, F. G. Pikus, P. M. Petroff, and A. L. Efros, Phys. Rev. B **55**, 1568 (1997).